Electrochimica Acta 313 (2019) 141–150

Contents lists available at ScienceDirect

Electrochimica Acta

journal homepage: www.elsevier.com/locate/electacta

# Fault detection for polymer electrolyte membrane fuel cell stack by external magnetic field

Lyes Ifrek [a, b], Sébastien Rosini [c], Gilles Cauffet [a], Olivier Chadebec [a], Luc Rouveyre [d], Yann Bultel [b, *]

[a] Univ. Grenoble Alpes, CNRS, Grenoble INP, G2Elab, F-38000 Grenoble, France
[b] Univ. Grenoble Alpes, Univ. Savoie Mont Blanc, CNRS, Grenoble INP, LEPMI, F-38000, Grenoble, France
[c] Univ. Grenoble Alpes, CEA, LITEN, F-38054, Grenoble, France
[d] SymbioFCell, F-38600, Fontaine, France

ARTICLE INFO

*Article history:*
Received 29 January 2019
Received in revised form
25 April 2019
Accepted 30 April 2019
Available online 7 May 2019

*Keywords:*
Fault detection
Non-invasive diagnosis
PEM fuel cell
Magnetostatic inverse problem
Current density identification

ABSTRACT

An original non-invasive approach of fuel cell diagnosis is proposed in order to locate different kinds of faults in PEMFC stacks from magnetic field measurements. The method is based on the solving of an inverse linear problem linking the magnetic field signature outside of the fuel cell to the current density distribution inside. The searched solution is a linear combination of conservative current distribution obtained by a set of electrokinetic problems solved by a finite face element method. As the problem is ill-posed, the solution is stabilized using a truncated singular value decomposition. In this work, 30 sensors are used to perform the magnetic tomography of a PEMFC stack consisting of 100 cells with a large active area of 220 $cm^2$. External magnetic measurement makes possible to identify 2D or 3D changes of current density distribution induced either by a cell flooding or membrane drying as well as by material degradation in a PEMFC stack.



## 1. Introduction

Of the many barriers currently impeding the deployment of Proton Exchange Membrane Fuel Cell (PEMFC), cost and durability represent two of the most significant challenges to achieve clean, reliable, and cost-effective PEMFC systems, in particular for automotive applications, where reliability and durability are critical. For mass integration of fuel cell systems in electric vehicles, the US DOE and European commission targets are only reached in terms of performances (2 kW $kg^{-1}$ and 2.25 kW $L^{-1}$), but neither in terms of durability (2500 h *vs* 5000 h) nor price (24 *vs* 20 $ $kWe^{-1}$), which is currently the main hurdle to massive development [1]. Solving these shortcomings will be a great opportunity for a decisive breakthrough towards mass-diffusion of the current PEMFC technology.

Regarding the reliability of the large PEMFC stack, one important problem to solve is the current heterogeneities existing at the cell surface level and along the stack length. These latter heterogeneities at the stack level may be induced by local operating conditions (flooding, drying, etc.) or material degradation. Indeed, Robin et *al.* [2] observed an important dispersion of the 30 cells voltages during the durability test of large area PEMFC stack. At the cell level, they observed heterogeneous current density distribution under dry and wet conditions due to the local conditions such as temperature, relative humidity, etc. Current density heterogeneities at the stack level may be related to local degradation of the Membrane Electrode Assembly (MEA) constitutive materials. Wu et *al.* [3] note a decrease of Gas Diffusion Layer (GDL) conductivity and hydrophobicity after fuel cell operation. Namely, Das et *al.* [4] showed that aged GDLs demonstrate higher adhesion forces, which dominate GDL degradation response and fuel-cell water holdup. The PTFE (hydrophobic agent) and carbon support are subjected to chemical attack and oxidation, leading to change in GDL properties. The main degradation mechanisms of Catalyst Layers (CL) are well demonstrated in the literature: (i) migration/aggregation of the Pt-based nanoparticles, (ii) corrosion of the carbon support, (iii) dissolution/redeposition of the Pt-based nanoparticles (3D Ostwald ripening) and (iv) chemical reduction of the $Pt^{z+}$ ions produced by Ostwald ripening [5,6]. It is now well accepted that membrane degradation is a combination of both mechanical and chemical

* Corresponding author.
*E-mail address:* yann.bultel@lepmi.grenoble-inp.fr (Y. Bultel).

https://doi.org/10.1016/j.electacta.2019.04.193
0013-4686/

degradation effects [7].

On the one hand, it is critical to develop inspection techniques able to measure local properties on every location on the sheet material such that defects in MEA components can be removed prior to assembly into complete PEMFC stack. Infrared thermography was proposed for rapid (with response times on the order of 1 s for large areas), noncontact, and nondestructive detection of defects [8,9]. On the other hand, it is also critical to develop techniques able to detect anomalies at the stack level during operation induced either by ineffective conditions or material defects induced by ageing [10]. Up to date, electrochemical techniques, such as polarization curve, current interruption, and electrochemical impedance spectroscopy (EIS), have been popularly employed for fuel cells diagnosis. Measurements of cell voltages are the simplest to perform and to (often) interpret voltage drops, indicating failures necessitating the immediate shutdown of the stack [11]. EIS is also a well-established diagnostic method [12–17] that has been widely used in electrochemistry due to its flexibility (which enables covering a wide range of aspects of fuel cells) and accuracy [12]. Routine experimental methods based on different techniques devoted to the evaluation of cell state (Cell voltage, polarization curve, EIS, etc.) are certainly powerful, but remain insufficient when dealing with the heterogeneous aspects of the ageing phenomena at stake in the cell [18] and even more within a stack. Indeed, owing to the cell geometry, the uniformity of the chemical, physical, and electrical values is never perfectly achieved. It is well-known that the local operating conditions in the stack depend on the position of the cell in the stack and over the cell surface because of the flow-field design [2]. Therefore, techniques allowing local measurement of PEMFC parameters at the stack level, are of major interest to sense localized ageing phenomena and understand degradation mechanisms. Namely, numerous in situ techniques have been developed to determine the current distribution over the cell surface [19–23]. This is generally performed by using "invasive probes" such as segmented cell to measure the current density distribution. Segmented cells are increasingly used for in situ investigation of PEMFC operation [24], for instance to design channels [25] or to optimize their performances [26] and are also suitable for the study of degradations [27,28]. At the stack scale, in situ current mapping on the active surface area can be assessed by the implementation of an S++® measurement device from the S++® Simulation Services Company [http://www.splusplus.com] within the stack [18]. Nevertheless, the S++® devices are large intrusive components, well-adapted to test bench studies but poorly applicable in real systems. Moreover, their maximal acquisition frequency is around 0.5 Hz which prevents any coupling of such S++® mapping with classical EIS characterizations. Lilavivat *et al.* [29] present an overview of techniques for mapping the current distribution within a fuel cell. More recently, Lee *et al.* [30] used micro-electro-mechanical systems (MEMS) technology to integrate micro temperature, voltage and current sensors into a 40 mm thick stainless steel substrate successfully. Despite their indubitable fundamental interest, these techniques (segmented cell, current mapping) cannot be deployed on a real PEMFC system. Moreover, these techniques allow only to give an information about the current density distribution at one cross sectional location in the stack while today a complete current density mapping along the stack length is required.

However, non-invasive methods based on measurements of the magnetic field induced by current production within the stack have been proposed in the literature and for PEMFC stack diagnosis [31,32]. The external magnetic field measurement is a new and original technique, which consists in placing magnetic sensors around the stack, to measure the magnetic field generated by the current flowing through it. Previously, magnetic field cartography has been performed using a 3-axis magnetic sensor displaced around the PEMFC stack via a moving sensor. 300 measurements were necessary to obtain a good resolution on the current distribution mapping [31]. Unfortunately, this acquisition lasts 15 min, a time during which the internal state of the fuel cell can vary and may lead to wrong current estimation. Moreover, such a system is extremely complex to develop and can only be used in a laboratory context. Yamanshi *et al.* [33] also investigated fuel cell diagnosis by measuring the magnetic field, and an additional study was done in Ref. [34]. In these studies, a genetic algorithm is used to find a linear combination of magnetic field signatures associated to elementary faults. The current density distribution is then reconstructed in a fuel cell containing only one MEA.

Previous work [35,36] have validated a method to determine the internal state of a PEMFC stack based on non-intrusive external magnetic measurements by comparison to those recorded by the S++ card. This new and innovative magnetic tomography approach was used in order to reconstruct faults in PEMFC stacks by using one sensor array in the middle of the stack. The originality of our approach is that it requires a very small number of magnetic field sensors while maintaining an acceptable resolution within a shorter delay than the 15 min with the previous methods [31,32]. The major advantage is that the internal state of the stack does not vary during the measurement time (i.e. 1 min). The low number of sensors is made possible thanks to assumptions on the current distribution and to an adequate choice of magnetic sensors location and orientation according to the stack dimensions. However, the diagnosis tool is designed to be sensitive only to current heterogeneities induced by global faults (2D Fault) which affect identically all the cells of the stack. To go further, this approach has been improved to be sensitive to more localized faults involving only few adjacent cells in a stack and by proposing an original 3D faults identification method. An inverse model of the Biot and Savart law was then developed, allowing the 3D reconstruction of current density in a fuel cell from external measurements of the magnetic field [37]. The developed tool is validated on a large PEMFC stack that consists of a stack of 100 cells with an active cell area of 220 $cm^2$ (Fig. 1). The faults, induced by using either tailored defective MEAs or thanks to specific operating conditions, are used to characterize how local and overall performances of the MEA are affected. In case of operating conditions faults configurations, flooding or drying may involve all the cells of the stack generally in the same zone. This anomaly is defined in the paper as a 2D fault. In the case of localized faults induced by material degradation, one cell or few cells may be involved. This anomaly is defined as a 3D fault in the paper. For automotive, this tool would be useful to locate faults induced by either inappropriate operating conditions or degraded areas inside a stack. Our target is to provide a magnetotomography of the current distribution inside a stack in real operation.

This works is organized in 3 parts. The first consists on a description of the experimental setup. The second focuses on the methodology build around virtual measurements (virtual electrokinetic and magnetic behaviors of the stack) in order to establish and solve the inverse problem and thus identify the current density distribution in a faulty stack. The third step presents the implementation of our method on faulty stacks.

## 2. Description of the experimental setup

### 2.1. PEMFC stack description

Magnetic measurement system was tested and validated on a stack that consists of 100 cells with an active area of 220 $cm^2$, connected in series from the GENEPAC technology (Fig. 1a) [18].

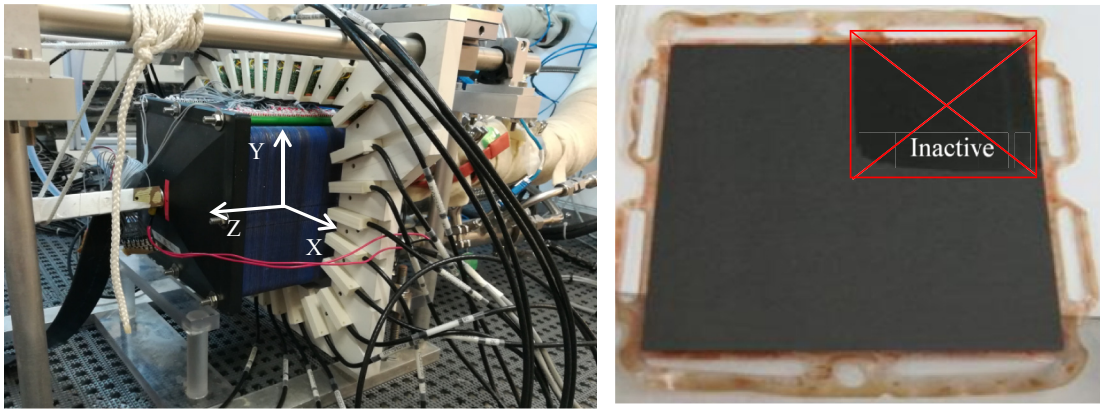


**Fig. 1.** Experimental setup: GENEPAC stack surrounded by a magnetic sensors array in laboratory environment (a) and MEA with 20% of the active area inhibited using resin (b).

Each cell is composed of one Membrane Electrode Assembly (MEA) where the electrochemical reactions take place and one bipolar plate with serpentine flow field. This latter is a multifunctional component, which ensures proper reactive gases distribution in the cell and product exhaust, separates the different cells of the stack, collects the current away from the cell, assists the heat and water management, and ensures the mechanical stability and sealing of the stack. The geometric characteristics of this fuel cell are given on Table 1.

The PEMFC stack was operated under conditions gathered in Table 2. These reference conditions are considered as a healthy mode for which the PEMFC stack shows stable current or voltage during a long period with a low performance decrease.

In order to mimic the operation of the stack in faulty modes, anomalies may be induced by either changing the operation conditions (air stoichiometry or air relative humidity) or introducing a localized fault by changing the properties of few MEA inside the stack. Indeed, set of measurements were made in order to validate the ability of our methodology to diagnose an evolution of internal stack operating conditions during oxygen starvation and membrane drying. Measurements were made using the following protocols:

- The stack was operated in healthy mode at least during 30 min in order to reach the steady state performances. Cell voltages and magnetic fields were recorded during this step.
- The studied parameter (inlet relative humidity or air stoichiometry) was changed and effects on stack voltage, cell voltages distribution and magnetic field was recorded during at least 1 h at constant current.
- The previous step was repeated for different air relative humidities, different air stoichiometries in order to map the effect of operating set point on voltages and on magnetic field.

**Table 1**
Geometrical parameters of the GENEPAC PEM fuel cell.

| | |
|---|---|
| Rectangular section | $0.164 \times 0.136\ m^2$ |
| MEA thikness | 0.43 mm |
| Bipolar plate thikness | 1 mm |
| End plate thikness | 2.5 mm |
| Fuel cell length | 148 mm |
| Distance sensor/Stack | 35 mm |
| Number of cells | 100 |

**Table 2**
Operating conditions during magnetic measurement corresponding to healthy mode.

| | |
|---|---|
| Air stoichiometry (Sto) | 2 |
| Hydrogen stoichiometry (Sto) | 1.5 |
| Air relative humidity (RH) | 80% |
| Hydrogen relative humidity (RH) | 80% |
| Anode pressure | 1.5 bar |
| Cathode pressure | 1.5 bar |
| Temperature | 80 °C |

During a third experiment, a set of measurements was made in order to validate the ability of the magnetic measurement method to identify a local fault within a PEMFC. This latter case was done to mimic a local MEA degradation (carbon corrosion, Platinum dissolution, etc.). To do this, the stack was disassembled and the cells 61 to 65 were extracted from the stack. 20% of the active surface of these 5 cells was covered with a resin that inhibits this area (Fig. 1b). Once the cells were reassembled within the fuel cell stack, new measurements were performed in reference conditions at the same current of I = 100 A.

### 2.2. Magnetic field device description

As shown in Fig. 1a. 30 sensors are positioned on the same plane perpendicularly to the current flowing. In order to maximize the signal to noise ratio, sensors are located as close as possible to the stack. This single array of sensors is moved along the stack length to perform measurements on three different locations along z-axis of the stack (Fig. 2) [37]. The sensors orientation is chosen in order to mainly measure the magnetic field due to the heterogeneity of the current density distribution [35]. That is to say that the orientation of the measurement axes of each sensor is defined in order to be insensitive to the main current flow through the stack. Thus, only the axial and radial components, $B_u$ and $B_w$, are used (Fig. 2b) because of their sensitivity to any heterogeneous current streamline distribution. On previous works [35] only one sensor array of 30 magnetic sensors was used, in the middle of the stack (middle sensor array Fig. 2a) and the identification of the current distribution was made only from radial magnetic component ($B_u$). In order to improve our method and apply it to local fault identification, three measurement locations are considered in this work as depicted in Fig. 2a. In practice, the sensors array is moved on the

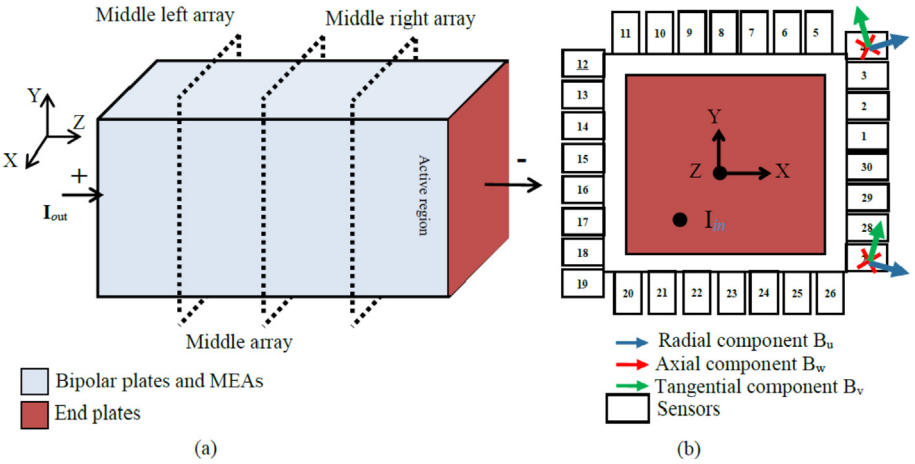


**Fig. 2.** Set-up sensor positions around the stack (a) and sensors locations for each array (b).

left, middle and on right position during experiments to record magnetic field in these three location (Fig. 2a).

## 3. Identification of the current density from the external magnetic field

It has been established that the current density distribution is modified by the operational process control mode [2]. The magnetic field depends on the current flowing through all the components of the stack and devices around it (active part of the stack, end plates, current collectors, and external connections to load and auxiliaries). A direct modeling based on the equations governing the electrokinetic then, the magnetostatic phenomena are used to define virtual or simulated magnetic measurements.

As the external magnetic field generated by the fuel cell is an image of the current density distribution in the stack, an inverse linear problem has to be solved. The first step for inverse problems solving is the parameterization of the causes (here is the current density distribution) and effect (magnetic field). The key point of the inverse modeling is the choice of the current density parameterization, which has to be sufficiently compact in order to limit the number of degrees of freedom, but also sufficiently large to cover the space of all possible faults configurations.

### 3.1. Direct problem

The electrokinetic model of the PEMFC stack is based on a previous physic-based approach [38]. This model is composed of multiple single repeat units stacked on top of each other and sandwiched between two end plates along the z-axis. The electrical behavior of the fuel cell is modelled using a Finite Element Method (FEM) and face shape functions as described in Ref. [39].

After the FEM electrokinetic resolution that leads to the current distribution on the mesh of the fuel cell, a magnetostatic problem has to be solved in order to compute the magnetic field at any point around the stack. It can be efficiently achieved by numerically integrating the Biot and Savart law (Eq. (1)):

$$\boldsymbol{B}(\boldsymbol{r}) = \frac{\mu_r}{4\pi} \int_{\Omega_s} \frac{(\boldsymbol{r_s} - \boldsymbol{r})}{|\boldsymbol{r_s} - \boldsymbol{r}|^3} \times \boldsymbol{j}(\boldsymbol{r_s}) d\Omega_s \quad (1)$$

where **B** the magnetic induction at position **r, j** the current density at the integrating point $\mathbf{r_s}$, $\Omega_s$ the stack volume and $\mu_r$ is the magnetic permeability of the air.

The geometrical parameters of a GENEPAC technology stack (Table 2) are considered to simulate the current density distribution as well as the streamline. The electrical conductivities of the heathy and faulty stacks are given in Table 3 [38]. Note that the healthy stack considers homogeneous conductivities while the faulty part of the stack assumes a conductivity close to zero. For numerical reason, the conductivity of the faulty zone is assumed equal to $1 \times 10^{-4} (\Omega \cdot m)^{-1}$.

The Fig. 3 shows the different type of simulated current density as well as the streamlines distribution on a slice in the middle of the fuel cell and along the stack length. The size of the current loop depends on the number of affected cells and the electrical conductivity ratio between the healthy and the faulty zones. Two cases of faults can be defined as global faults called also 2D fault (Fig. 3a1) or localized faults called also 3D fault (Fig. 3a2). In case of operating conditions faults configurations, flooding or drying (2D fault) may involve all the cells of the stack generally in the same zone. This ideal case assumes the same fault on all cells along the stack in the lower part. In that case, the current density is forced to pass through the upper part (Fig. 3a1). Subtracting the healthy, which assumes homogeneous simulated current streamline distribution in the active part and the main current in the fuel cell flows along the **z**-axis (Fig. 3b1), the current density loop, therefore, covers all the length of fuel cell (Fig. 3c1). In case of localized faults induced by material degradation (3D fault), one cell or few cells may be involved as shown in Fig. 3a2. Subtracting the healthy mode (Fig. 3b2), the current density loop (Fig. 3c2) is located on the left part of the stack and involves only the cells affected by the fault and its neighbors. For each current distribution (healthy, faulty and differential), the dedicated magnetic field can be calculated using the Biot and Savart law's (Eq. (1)).

As shown on the case of a 3D fault (Fig. 3a2), any current distribution (Fig. 4a) can be described as the sum of a healthy mode (Fig. 4b) plus a simple current loop (Fig. 4c). So, let us take as an example a faulty fuel cell. We assume that any current density distribution can be decomposed into a healthy mode and a current density loop on the yz-plane. We conclude that the current density

**Table 3**
Stack electrical conductivity parameters $(\Omega \cdot m)^{-1}$ [38].

| | Healthy case | Faulty case |
|---|---|---|
| Bipolar plate + MEAs average conductivity | $5 \times 10^3$ | $1 \times 10^{-4}$ |
| End plate conductivity | $5 \times 10^7$ | $5 \times 10^7$ |

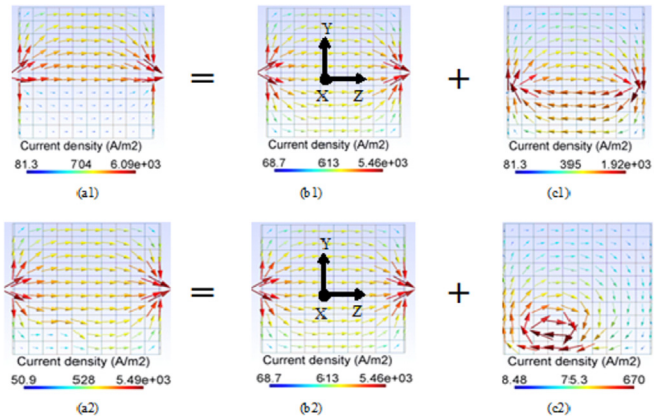


**Fig. 3.** Decomposition of a simulated current distribution for two kinds of faults (2D and 3D) on a slice in the middle of the fuel cell and along the stack length: Decomposition of a 2D fault current (a1) into a sum of a healthy mode current (b1) and a current loop induced by a fault (c1); Decomposition of a 3D fault current (a2) into a sum of healthy mode current (b2) and a current loop induced by a fault (c2).

distribution basis should contain a set of current loop configurations [37]. This approach has been already used by Le Ny *et al.* [35,36].

### 3.2. Choice of the current density distribution parametrization

According to our description, the current density difference $\Delta\mathbf{j}$ (Fig. 4c), is a current loop defined as:

$$\Delta\mathbf{j} = \mathbf{j}(\mathbf{faulty}) - \mathbf{j}(\mathbf{healthy}) \tag{2}$$

where $\mathbf{j}$ (**faulty**) (Fig. 4a) is the current density for a faulty stack and $\mathbf{j}$ (**healthy**) (Fig. 4b), the one for a healthy stack.

As an assumption, any distribution of the current density difference $\Delta\mathbf{j}$ can be expressed as a linear relation of $\Delta\mathbf{j_i}$where $\Delta\mathbf{j_i}$ corresponds to current density difference due to an elementary loop as shown on Fig. 4c. In that case, the $\Delta j$ is given by:

$$\Delta\mathbf{j} = \sum_{\mathbf{i}} \mathbf{I_i}\Delta\mathbf{j_i} \tag{3}$$

where $I_i$ is the contribution coefficient of the $\Delta\mathbf{j_i}$ vector to the current density difference $\Delta\mathbf{j}$.

In order to define the $\Delta\mathbf{j_i}$ differences, the fuel cell stack domain is divided into $5 \times 5 \times 5$ vol parts. A zero electrical conductivity is imposed on each part separately to get a basis of 125 elementary faults and thanks to FEM electrokinetic model, the current density distribution inside the fuel cell is obtained. For each configuration, the healthy current density is subtracted to get only the current loop due to the fault. The Fig. 5 shows 4 examples of current density differences among the 125 simulations. Based on this approach, we assume that any current density difference induced by either a 2D fault (Fig. 3c1) or a 3D fault (Fig. 3c2) can be decomposed as a sum

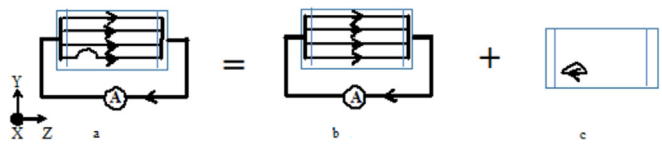


**Fig. 4.** Theoretical decomposition of a heterogeneous current (a) healthy mode current (b) and current loop induced by a fault (c) on a cross-section along the stack length for a 3D fault.

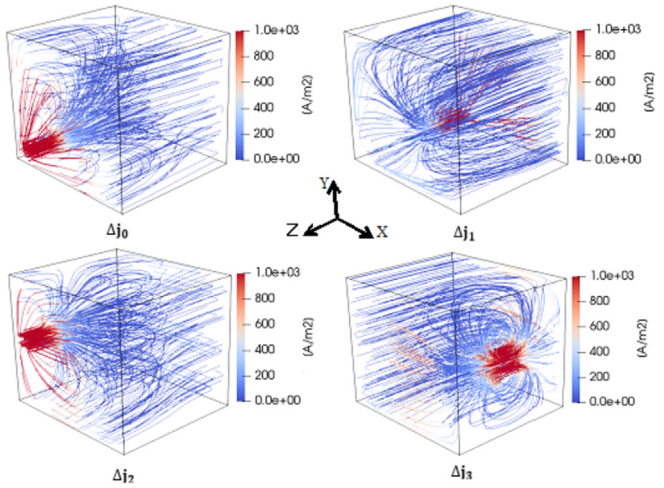


**Fig. 5.** Example of four vectors used to build the current basis.

of this 125 current density difference as expressed in Eq. (3). We make the assumption that these 125 elementary current vectors can cover the space of all possible faults configurations.

### 3.3. Choice of the magnetic field parametrization

Knowing this current basis, a magnetic field basis could be defined by integrating Biot and Savart law:

$$\Delta B_k = \frac{\mu_0}{4\pi}\sum_i I_i u_k \cdot \int_{\Omega} \frac{r}{r^3} \times \Delta j_i \, d\Omega \tag{4}$$

where $\Delta B_k$ is the magnetic field difference between the faulty and the healthy case at sensor $k$ generated by a current density difference $\Delta\mathbf{j_i}$ between a faulty and healthy mode and $\mathbf{u_k}$ the orientation of the sensor $k$.

For example, Fig. 6 presents four magnetic field magnitudes corresponding to four elementary current loops shown on Fig. 5 on the 3 magnetic sensor arrays.

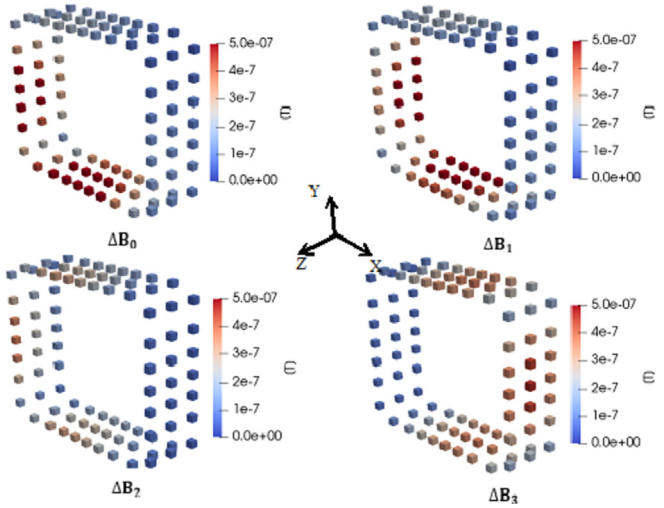


**Fig. 6.** Example of four vectors used to build the magnetic basis: Magnetic field magnitude vectors related to current vectors (Fig. 5).

### 3.4. Inverse model

Equation (4) has been written for one sensor. By considering all the sensors, a linear relation linking the magnetic field on sensors and current density vectors can be obtained:

$$\Delta\mathbf{B} = \mathbf{S}\Delta\mathbf{J} \tag{5}$$

where $\mathbf{S}$ is the discretized Biot and Savart operator, $\Delta\mathbf{B}$ is the measurement difference vector and $\Delta\mathbf{J}$ is the current density difference vector.

It remains to solve this system to reconstruct the current density difference distribution $\Delta\mathbf{J}$. These inverse problem is said to be ill-posed [40], meaning that its solution is not unique. A good solution is to compute the pseudo inverse $\mathbf{S}^{+}$ of $\mathbf{S}$ based on the Singular Value Decomposition (SVD) which can be truncated in order to limit the influence of measurement noise. This distribution can be finally obtained by solving [41]:

$$\Delta\mathbf{J} = \mathbf{S}^{+}_{\mathbf{trc}}\Delta\mathbf{B} \tag{6}$$

where $\mathbf{S}^{+}_{\mathbf{trc}}$ is the truncated pseudo inverse of the operator $\mathbf{S}$.

## 4. Experimental Results

The developed approach is deployed on a real stack in a laboratory environment for which anomalies are induced by either changing the operation conditions (2D fault) or by introducing a localized fault (3D fault).

### 4.1. Identification of a global 2D fault

Two examples of the evolution of averaged cell voltage with operating conditions are depicted on Fig. 7. Firstly, the evolution of averaged cell voltage and cell voltage standard deviation obtained on a healthy stack when the air stoichiometry is decreased from 2 down to 1.3, are shown in Fig. 7a for a nominal current equals to 100 A. Except air stoichiometry, all operating parameters are equals to parameters in the reference conditions (Table 2). As expected due to mass transport limitations, the decrease of air stoichiometry induces a decrease of the averaged cell voltages from 0.72 to 0.7 V whereas no important evolution of the cell voltages standard deviation (from $2.10^{-3}$ to $5.10^{-3}$ V approximately, corresponding to a difference between maximum and minimum cell voltages equals to 20 mV) is observed indicating that no important heterogeneities are induced along the stack. Nevertheless, it is worth mentioning that the cell voltages become more and more unstable for the lower air stoichiometry because of the $O_2$ starvation. The second case deals with the evolution of the current distribution and of the average cell voltages with respect to relative humidity. The evolution of averaged cell voltage of the stack and cell voltage standard deviation for air relative humidity from 80% down to 30% and for I = 100 and 50 A are depicted in Fig. 7b. As expected, the voltage increases when air relative humidity rises due to membrane humidification. Once again, no important discrepancy is observed in individual cell voltages and cell voltage standard deviation remains below 10 mV during experiment. As a consequence, it can be concluded that modification of inlet relative humidity seems to have the same effect to each cells along the stack.

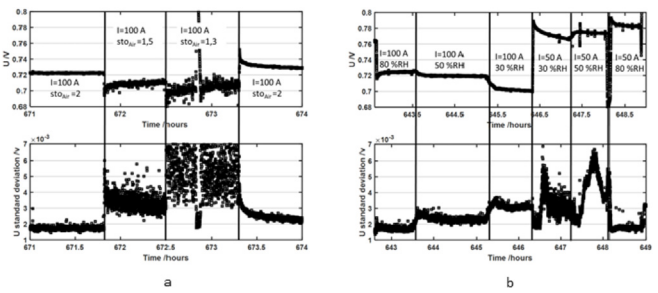


**Fig. 7.** Effect of the air stoichiometry variation at I = 100 A (a) and effect of the air relative humidity variation at I = 100 A and I = 50 A (b) on the evolution of average cell voltages as a function of time.

The magnetic field measurement on the three sensor arrays were recorded for the different air stoichiometry and air relative humidity. To obtain information about current distribution evolution with the stack input parameters, magnetic field evolution $\Delta\mathbf{B}$ is calculated for each measurements using the difference between the magnetic field recording in **"healthy"** conditions and magnetic field recording in **"faulty"** conditions. We consider that fuel cell working in reference conditions (Table 2) is supposed as a **"healthy"** stack while the stack working at lower stoichiometry (1.5 and 1.3) and relative humidity (50% and 30%) is assumed as a **"faulty"** one:

$$\Delta\mathbf{B} = \mathbf{B}(\mathbf{faulty}) - \mathbf{B}(\mathbf{healthy}) \tag{7}$$

$\Delta\mathbf{B}$ is used in order to calculate the corresponding distribution of the current density difference $\Delta\mathbf{J}$ (Eq. (2)) for each value of air stoichiometry and air relative humidity. The results are presented in Fig. 8 when the air stoichiometry drops from 2 down to 1.3. On Fig. 8a, the change of current density distribution in the middle of the stack when comparing a "healthy" (sto = 2) to a "faulty" (sto = 1.5) is shown with the arrows displaying the location of the air inlet and air outlet and the design of gas flow fields. For air stoichiometry decreasing from 2 down to 1.5, the heterogeneity of the current density rises due to oxygen starvation from inlet to outlet for mean current density of 0.5 A/cm$^2$. An increase of the current density is observed at the air inlet (+0.1 A cm$^{-2}$) while a decrease is obtained at the air outlet (−0.1 A cm$^{-2}$). This current density distribution obtained from our inverse problem resolution is in agreement with previous measurements obtained using an internal measurement device located in the center of a fuel cell stack in operation [36].

Using a 3 dimensional magnetic description in addition to measurements in the middle of the stack make it possible to capture the current density changes at different locations within the fuel cell. As an example, Fig. 8b, shows the current density modification, with respect to the current density at reference conditions, for an air stoichiometry equals to 1.5 and on the cross sections, located on the left, middle and right sides of the stack. Whatever the location in the stack, the heterogeneity of the current density rises due to oxygen starvation from inlet to outlet for mean current density of 0.5 A/cm$^2$ when air stoichiometry decreases from 2 down to 1.5. Nevertheless, the identified current density changes are not exactly the same for the 3 cross sections. The current density changes are higher in the middle of the stack than on the left and right sides. This phenomenon is likely due to the current homogenization by the end plates and the current collection. The current density modifications on the three previous cross section for an air stoichiometry equals to 1.3 and when the stoichiometry is fixed to the initial value of 2, as in reference conditions, are respectively shown on Fig. 8c and d. As expected, operation at lower stoichiometry than 1.5 induces an increase of the current density at the air inlet in agreement with the modification of the gases activity along the active surface and the same phenomena of current distribution observed along the stack for a stoichiometry equals to 1.5 are recorded for lower stoichiometry. In addition, the current density difference recorded at the end of the experiment with a

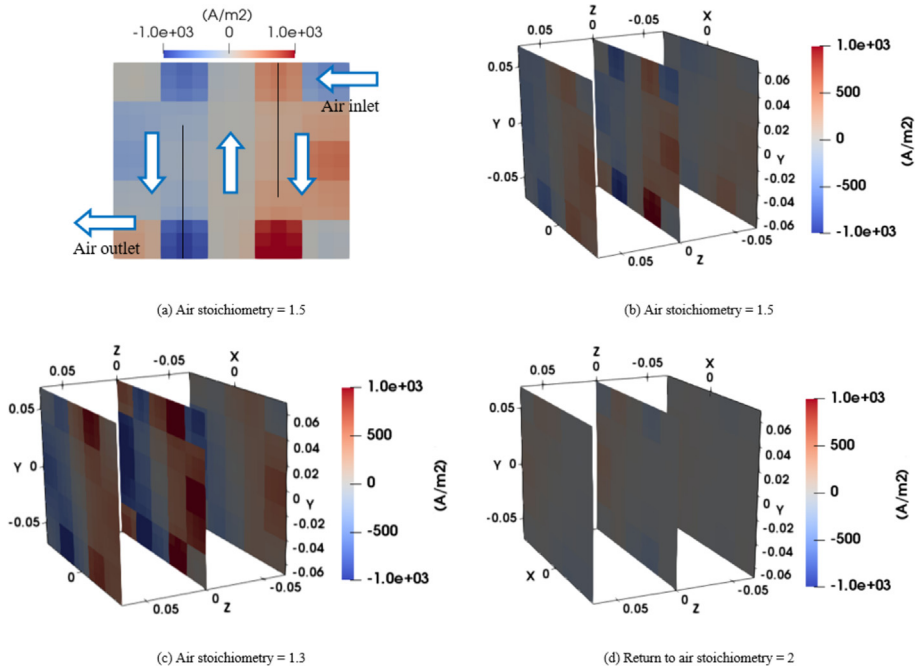


**Fig. 8.** Identified current density changes ($\Delta \mathbf{J}$) from magnetic field measurement for air stoichiometry ranging from 2 down to 1.5 for the middle cross section (a) and for the left, middle and right cross sections (b); from 2 down to 1.3 for the left, middle and right cross sections (c) and return to 2 for the left, middle and right cross sections (d).

stoichiometry equals to the reference stoichiometry are close to zero indicating that the stack remains to its original state after experiment.

The model was also used to identify current density changes during membrane drying/humidification when the air relative humidity varies (Fig. 7b). The Fig. 9a shows the change of current density distribution in the middle of the stack comparing a stack working in dry condition (air relative humidity 30%) to the healthy one (reference condition). Contrary to the previous case, lower current density is observed close to the air inlet meanwhile larger current density is obtained close to the gas outlet when the stack is working under dry condition (air relative humidity 30%) compared to the healthy stack. The effect is clearly related to the high water removal process at the inlet part of the cell and to progressive hydration of the membrane along the channel because of water production by an oxygen reduction reaction at the cathode.

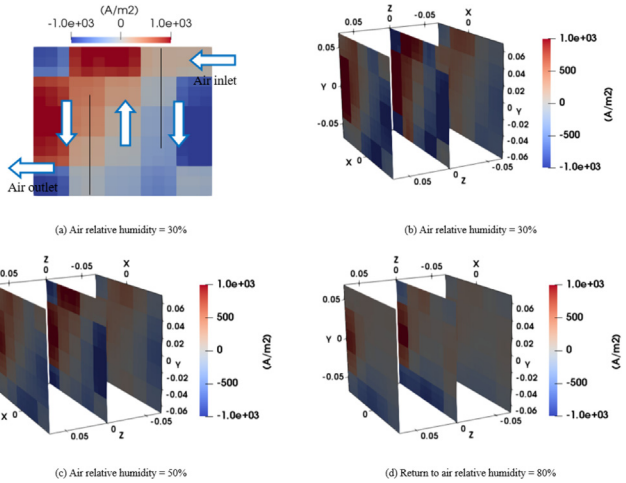


**Fig. 9.** Identified current density changes ($\Delta \mathbf{J}$) from magnetic field measurement for air relative humidity ranging from 80% down to 30% for the middle cross section (a) and for the left, middle and right cross sections (b); from 80% down to 50% for the left, middle and right cross sections (c) and return to 80% for the left, middle and right cross sections (d).

Fig. 9b,c,d show cross sections, located on the left and right sides of the stack as well as in the middle. The identified change of current density distributions become more and more homogeneous when air relative humidity rises from 30% to 80%. The current density modifications are again higher in the middle of the stack than on the left and right sides (Fig. 9b and c).

As a conclusion, the magnetic model developed in this work is sensitive to current density change induced by modification of operating conditions all along the stack as illustrated by water flooding or membrane drying underwent experiments. Moreover, on contrary to previous work [35] and according the assumptions used to build 3D magnetic model, it should be the able to identify a fault (3D faults) located only in a part of the fuel cell stack.

## 4.2. Identification of a local 3D Fault.

In order to validate the ability of the magnetic measurement method to identify a local fault within a PEMFC, a last set of measurements was made with stack containing five neighboring MEAs with 20% of active surface area inhibited (Fig. 1b).

The magnetic field on the three sensor arrays for the healthy case (i.e. nominal condition at a current I = 100 A) and the faulty stack are measured and, the magnetic field difference calculated according to Eq. (7), is shown in Fig. 10. In that case, the shape of the field is not identical on the three sensor arrays because of the location of the 3D fault. This result suggests that the current distribution is heterogeneous over the entire stack length. It is worth mentioning that the differential signature of the magnetic field generated by this fault is greater on the radial component of the left sensor plane and it is of the order of 40 μT. This indication makes it possible to conclude that the fault is strictly 3D and located on the left side of the stack.

Fig. 11a shows individual cell polarization curves obtained with


**Fig. 10.** Magnitude of the magnetic field for the 3D Fault (Bu: Radial component and Bw: Axial component).

stack containing five neighboring MEAs with 20% of active surface area inhibited. As expected, the fives cells affected by the 3D fault exhibits the lowest performances. At the same time, the unmodified MEAs have the same electrical characteristics except the cell n°66, which is located close to the faulty cells. It seems to have slightly better performances than the other cells. This behavior has already been simulated and seems to be due to a constriction phenomenon of the current streamlines in the vicinity of a fault [38].

The current density difference is then calculated according to Eq. (6) and is shown in Fig. 11b. The distribution of current density difference is very heterogeneous in the plane crossing the fault (left cross section). Indeed, the current density is highly modified because the overall current is forced to pass through the healthy part of the cells. So, the current density becomes likely close to zero in the inactive MEA area (right top corner) and because of the current conservation, the current density is higher in the healthy zone. On contrary, the distribution of current density difference for healthy cells located far away from the faulty zone are very weak (right cross section). Indeed, cells located far away from the fault exhibits no change of current density due to the current redistribution by the bipolar plate [38]. Our diagnosis device is also sensitive to any current density change on the 3 cross sections induced by a localized fault underwent by only 5 cells of the stack.

## 5. Conclusion

In this paper, a non-invasive magnetic tomography approach was proposed in order to locate different kinds of faults in PEMFC stacks from non-invasive magnetic field measurements. A sensor array was developed and designed to be sensitive only to current heterogeneities using a few magnetic sensors with a high sensitivity and high dynamic located on three sections around the stack. The experimental results obtained on the GENEPAC stack show the sensitivity of the magnetic field to any change in operating conditions and to a localized fault on some cells of the stack.

The sensitivity of our diagnosis tool has been demonstrated for cell flooding and membrane drying by varying the air stoichiometry and air relative humidity respectively. The results obtained concord with those presented in previous works and confirm the interest of the magnetic measurement to identify stack operating mode variation. To go further, a local fault on five neighboring cells in the stack was identified with our diagnosis tool. The distribution of current density is highly modified on these cells and this has been clearly observed on the cell magnetic signature. The inversion of this signature of the magnetic field measurement allows the reconstruction of a heterogeneous current with lowered current densities on the inactive zone of the cells.

Significant gains on maintenance costs and lifetime of the fuel cell system can be achieved through a better estimation of the fuel cell state as well as a better control of operating conditions. This knowledge of the state of health of a fuel cell involves the development of methods and diagnostic tools that are non-invasive and have the lowest possible cost. External magnetic measurement makes possible the identification of 2D and 3D current distributions in the fuel cell independently of the size of the fault within the

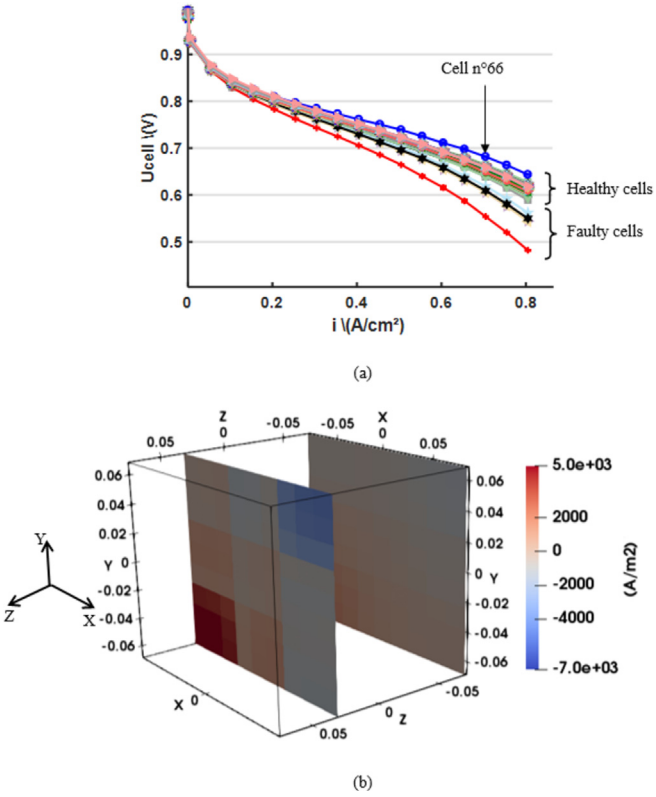


**Fig. 11.** Effect of 3D fault on individual cell polarization curves under reference conditions (a) and identified current density changes ($\Delta \mathbf{J}$) from the external magnetic field measurement (b).

limit of the precision of the sensors (resolution). In perspective, local electrochemical measurement may support stack-level degradation analyses as well as effective control to mitigate the consequences of degradation due to load cycles (electrochemical, thermal, mechanical and humidity effects) or faults. This research is a prerequisite to the stage of diagnosis, prognosis. It could lead to development of Fault Tolerant Control. A better estimation of fuel cell health and better control of operating conditions within the system would reduce maintenance costs and significantly increase its lifespan. Moreover, conclusions on interaction between design and heterogeneous current density should lead to specifications for stack design, as well as observation of interaction between the cells inside a stack. It should lead to the development of new generations for more robust stacks with an optimized design.

## Acknowledgement

Authors would like the Auvergne-Rhône-Alpes region for funding this work. This work is also supported by a public grant overseen by the French National Research Agency (ANR-17-CE05-0003-01 - LOCALI).

## References

[1] www.uscar.org, USDRIVE, Driving Research and Innovation for Vehicle Efficiency and Energy Sustainability: Technical Roadmap, 2016.
[2] C. Robin, M. Gérard, M. Quinaud, J. D'Arbigny, Y. Bultel, Proton exchange membrane fuel cell model for 220 predictions: simulated equivalent active surface area loss and comparisons with durability tests, J. Power Sources 326 (2016) 417–427.
[3] J. Wu, X.Z. Yuan, J.J. Martin, H. Wang, J. Zhang, J. Shen, S. Wu, W. Merida, A review of pem fuel cell durability: degradation mechanisms and mitigation strategies, J. Power Sources 184 (2008) 104–119.
[4] P.K. Das, A. Grippin, A. Kwong, A.Z. Weber, Liquid-water-droplet adhesion-force measurements on fresh and aged fuel-cell gas-diffusion Layers, J. Electrochem. Soc. 159 (2012) B489–B496.
[5] E. Guilminot, A. Corcella, M. Chatenet, F. Maillard, F. Charlot, G. Berthomé, C. Iojoiu, J.Y. Sanchez, E. Rossinot, E. Claude, Membrane and active layer degradation upon proton exchange membrane fuel cell steady-state operation - Part I: platinum dissolution and redistribution within the membrane Electrode assembly, J. Electrochem. Soc. 154 (2007) B1106–B1114.
[6] S. Maass, F. Finsterwalder, G. Frank, R. Hartmann, C. Merten, Carbon support oxidation in PEM fuel cell cathodes, J. Power Sources 176 (2008) 444–451.
[7] S. Kreitmeier, G.A. Schuler, A. Wokaun, F.N. Buchi, Investigation of polymer electrolyte membrane degradation in PEMFC using local gas permeation analysis, J. Power Sources 212 (2012) 139–147.
[8] N.V. Aieta, P.K. Das, A. Perdue, G. Bender, A.M. Herring, A.Z. Weber, M.J. Ulsh, Applying infrared thermography as a quality-control tool for the rapid detection of polymer-electrolyte-membrane-fuel-cell catalyst-layer-thickness variations, J. Power Sources 211 (2012) 4–11.
[9] P.K. Das, A.Z. Weber, G. Bender, A. Manak, D. Bittinat, A.M. Herring, M.J. Ulsh, Rapid detection of defects in fuel-cell electrodes using infrared reactive-flow-through technique, J. Power Sources 261 (2014) 401–411.
[10] C. Cadet, S. Jemei, F. Druart, D. Hissel, Diagnostic tools for PEMFCs: from conception to implementation, Int. J. Hydrogen Energy 39 (2014) 10613–10626.
[11] Z. Li, R. Outbib, S. Giurgea, D. Hissel, Y. Li, Fault detection and isolation for Polymer Electrolyte Membrane Fuel Cell systems by analyzing cell voltage generated space, Appl. Energy 148 (2015) 260–272.
[12] S. Niya, M. Hoorfar, Study of proton exchange membrane fuel cells using electrochemical impedance spectroscopy technique - a review, J. Power Sources 240 (2013) 281–293.
[13] N. Fouquet, C. Doulet, C. Nouillant, G. Dauphin-Tanguy, B. Ould-Bouamama, Model based PEM fuel cell state-of-health monitoring via ac impedance measurements, J. Power Sources 159 (2006) 905–913.
[14] S. Rodat, S. Sailler, F. Druart, P.X. Thivel, Y. Bultel, P. Ozil, EIS measurements in the diagnosis of the environment within a PEMFC stack, J. Appl. Electrochem. 40 (2010) 911–920.
[15] S. Tant, S. Rosini, P.X. Thivel, F. Druart, A. Rakotondrainibe, T. Geneston, Y. Bultel, An algorithm for diagnosis of proton exchange membrane fuel cells by electrochemical impedance spectroscopy, Electrochim. Acta 135 (2014) 368–379.
[16] S.K. Roy, H. Hagelin-Weaver, M.E. Orazem, Application of complementary analytical tools to support interpretation of polymer-electrolyte-membrane fuel cell impedance data, J. Power Sources 196 (2011) 3736–3742.
[17] N.V. Dale, M.D. Mann, H. Salehfar, A.M. Dhride, T. Han, Ac impedance study of a proton exchange membrane fuel cell stack under various loading conditions, J. Fuel Cell Sci. Technol. 7 (2010), 031010.
[18] F. Nandjou, J.P. Poirot, M. Chandesris, J.F. Blachot, C. Bonnaud, Y. Bultel, Impact of heat and water management on proton exchange membrane fuel cells degradation in automotive application, J. Power Sources 326 (2016) 186–192.
[19] J. Stumper, S.A. Campbell, D.P. Wilkinson, M.C. Johnson, M. Davis, In-situ methods for the determination of current distributions in PEM fuel cells, Electrochim. Acta 43 (1998) 3773–3783.
[20] M. Schulze, E. Gulzow, S. Schonbauer, T. Knori, R. Reissner, Segmented cells as tool for development of fuel cells and error prevention/prediagnostic in fuel cell stacks, J. Power Sources 173 (2007) 19–27.
[21] G. Maranzana, C. Moyne, J. Dillet, S. Didierjean, O. Lottin, About internal currents during start-up in proton exchange membrane fuel cell, J. Power Sources 195 (2010) 5990–5995.
[22] D. Candusso, J.P. Poirot-Crouvezier, B. Bador, E. Rullière, R. Soulier, J.Y. Voyant, Determination of current density distribution in proton exchange membrane fuel cells, Eur. Phys. J. Appl. Phys. 25 (2010) (2004) 67–74.
[23] S. Sailler, S. Rosini, M.A. Chaib, J.Y. Voyant, Y. Bultel, F. Druart, P. Ozil, Electrical and thermal investigation of a self-breathing fuel cell, J. Appl. Electrochem. 37 (2007) 161–171.
[24] L.C. Pérez, L. Brandão, J.M. Sousa, A. Mendes, Segmented polymer electrolyte membrane fuel cells" - a review, Renew. Sustain. Energy Rev. 15 (2011) 169–185.
[25] M. Reum, S.A. Freunberger, A. Wokaun, F.N. Büchi, Measuring the current distribution with sub-millimeter resolution in PEFCs, J. Electrochem. Soc. 156 (2009) B301–B310.
[26] M. Reum, A. Wokaun, F.N. Büchi, Measuring the current distribution with submillimeter resolution in PEFCs III. Influence of the flow field geometry, J. Electrochem. Soc. 156 (2009) B1225–B1231.
[27] F.B. Weng, C.Y. Hsu, C.W. Li, Experimental investigation of PEM fuel cell aging under current cycling using segmented fuel cell, Int. J. Hydrogen Energy 35 (2010) 3664–3675.
[28] L. Dubau, L. Castanheira, M. Chatenet, F. Maillard, J. Dillet, G. Maranzana, S. Abbou, O. Lottin, s, A. El Kaddouri, C. Bas, L. Flandin, E. Rossinot, N. Caqué, Carbon corrosion induced by membrane failure: the weak link of PEMFC long-term performance, Int. J. Hydrogen Energy 39 (2014) 21902–21914.
[29] V. Lilavivat, S. Shimpalee, J.W. Van Zee, H. Xu, C.K. Mittelsteadt, Current distribution mapping for PEMFCs, Electrochim. Acta 174 (2015) 1253–1260.
[30] C.-Y. Lee, Y.-C. Chiang, F.-B. Weng, S.-C. Li, P.-H. Wu, H.-I. Yueh, Flexible micro temperature, voltage and current sensors for local real-time microscopic diagnosis inside high temperature proton exchange membrane fuel cell stack, Renew. Energy 108 (2017) 126–131.

[31] K.H. Hauer, R. Potthast, T. Wüster, D. Stolten, Magnetotomography: a new method for analysing fuel cell performance and quality, J. Power Sources 143 (2005) 67–74.
[32] H. Lustfeld, M. Reißel, B. Steffen, Magnetotomography and electric currents in a fuel cell, Fuel Cells 4 (2009) 474–481.
[33] R. Yamanashi, Y. Gotoh, M. Izumi, T. Nara, Evaluation of generation current inside membrane Electrode assembly in polymer electrolyte fuel cell using static magnetic field around fuel cell, ECS Transactions 65 (2015) 219–226.
[34] T. Nara, M. Koike, S. Ando, Y. Gotoh, M. Izumi, Estimation of localized current anomalies in polymer electrolyte fuel cells from magnetic flux density measurements, AIP Adv. 6 (2016), 056603.
[35] M. Le Ny, O. Chadebec, G. Cauffet, J.M. Dedulle, Y. Bultel, S. Rosini, Y. Fourneron, P. Kuo-Peng, Current distribution identification in fuel cell stacks from external magnetic field measurements, IEEE Trans. Magn. 49 (2013) 1925–1928.
[36] M. Le Ny, O. Chadebec, G. Cauffet, S. Rosini, Y. Bultel, PEMFC stack diagnosis based on external magnetic field, measurements, J. Appl. Electrochem. 45 (2015) 667–677.
[37] L. Ifrek, G. Cauffet, O. Chadebec, Y. Bultel, R. Rosini, L. Rouveyre, 2D and 3D fault basis for fuel cell diagnosis by external magnetic field measurements, Eur. Phys. J. Appl. Phys. 79 (2) (2017) 20901.
[38] M. Le Ny, O. Chadebec, G. Cauffet, J.M. Dedulle, Y. Bultel, A three dimensional electrical model of PEMFC stack, Fuel Cells 12 (2012) 225–238.
[39] T.T. Nguyen, G. Meunier, J.M. Guichon, O. Chadebec, T.S. Nguyen, An integral formulation for the computation of 3-D eddy current using facet elements, IEEE Trans. Magn. 50 (2014) 549–552.
[40] J. Hadamard, Lectures on Cauchy's Problem in Linear Partial Differential Equations, Yale University Press, 1923.
[41] P. Xu, Truncated SVD methods for discrete linear ill-posed problems, Geophys. J. Int. 135 (1998) 505–514.